# ALMA Memo 544

# Quasi-Optical Verification of the Band 9 ALMA Front-End

M. Candotti*, A. M. Baryshev†, N. A. Trappe*, R. Hesper†,
J. A. Murphy*, J. Barkhof†, W. Wild†.

*National University of Ireland, Maynooth, Co. Kildare, Ireland
Email: Massimo.Candotti@nuim.ie
†SRON (Netherlands Institute for Space Research), NOVA (Netherlands Research School for Astronomy)
and Kapteyn Astronomical Institute, 9700 AV Groningen, The Netherlands
Email: A.M.Baryshev@sron.rug.nl

$10^{th}$ of November 2005

**Abstract**

The front-end optical design for band 9 (600 to 720GHz) of the Atacama Large Millimeter Array (ALMA) is now completed and verified. A frequency independent design approach is used to couple radiation to the two orthogonal polarized mixed detectors from the large 12m ALMA Cassegrain telescope. As it is a heterodyne receiver, two local oscillator beam paths are integrated into the front-end optical system. Due to the large number of interferometer elements (64 antenna units) to be built, installed and maintained in the remote site of the Atacama Desert, reliability of the optical system should be ensured. A modular and compact optical design is also important. In addition a cheaper fabrication process is considered, at these more tolerant higher frequencies, by milling the mirror surfaces near the surface roughness limit. In this paper we verify the optical design and estimate system efficiency by means of experimental measurement and software simulation comparisons. Precision planar scans of near field beam patterns (amplitude and phase) have been measured. Experimental beam measurements were taken at the output of the mirror coupling system (telescope focal plane location) for both polarization paths and for both local oscillator beam guides. At the same measurement locations, software simulations of a highly accurate geometrical model of the mirror coupling system were predicted using the commercial package GRASP8©. These comparisons at some fundamental locations along the beam paths, allow the assessment of the quasi-optical beam coupling system design. The local oscillator power budget analysis is carried out from results obtained using GRASP8©. In the conclusion we summarize the current status and describe future analysis plans.

## I. Introduction

The work presented in this paper is a continuation of the optical design and later verification of the optical coupling mirror system for the ALMA band 9 system. This activity has started with the evaluation of a basic prototype of a two mirror coupling system [1], resembling the real optical design. In this initial work most of the attention was aimed at the evaluation of the mirror surface milling technique adopted. In fact, in order to minimize costs and improve system modularity, a a minimum surface roughness accuracy of $7\mu m$ RMS was choose and obtained with conventional CNC machines. By means of experimental measurements and later on also with software electromagnetic analysis [2], it was proven that these mechanical project choices were satisfactory operation of band 9. In phase one of the analysis the conceptual design was verified completely. Tight distance tolerances of $40\mu m$ were chosen to insure the optimum optical component alignment without the need for optical alignment with a laser beam. In this paper we then analyze measured and simulated data of the final optical coupling system to be mounted in to the band 9 cryostat, but at the room temperature. In section II we present a brief description of the optical coupling system project. The interested reader could have more information on this topic by reading [3]. Sections III and IV will describe respectively the measurement setup used to scan intensity and phase of the near field at the focal plane (FP) location and the electromagnetic software model implemented in GRASP8©. Measured data at two different frequencies (606 and $668GHz$) are then compared and analyzed with related software predictions at the same frequencies and location in section V. In this section a Gaussian Beam Mode Analysis (GBMA) is also carried out for the Co-Polar (Co-P) components. Due to the excellent agreement between measured (experimental) and software (theoretical) data is it then possible to make some system performance predictions using the simulation tool. An example is reported in section VI dealing with the Local Oscillator (LO) power budget requirements. Further work and conclusions are considered in section VII. A complete set of plots depicting all the measurements carried out during this campaign is reported in section VIII comparing them with the simulation results.

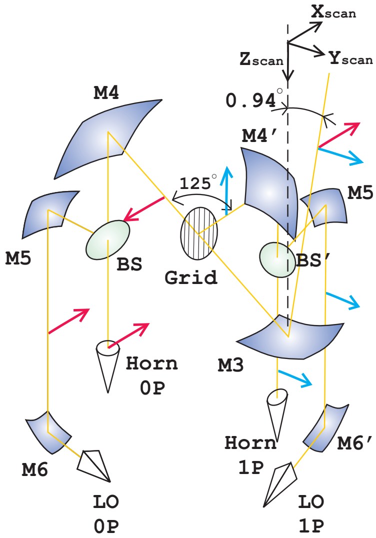


Fig. 1. Sketch of the optical coupling system for ALMA band 9.

## II. Optical coupling system

The telescope has to be coupled to the mixer corrugated horn with an illumination edge taper of $12dB$ at the secondary reflector. A series of two ellipsoidal mirrors were designed in order to refocus the horn field distribution twice and achieving the desired edge taper. Since there are two orthogonal linear polarized signals detected from the sky, the coupling system is in fact exactly duplicated for both of the two polarization channels. This is also the case of the LO signal injection system. The procedure used to design all the optics for this coupling system is based on geometrical optics techniques. The choice of the bending angles for the mirrors coupling the horn to the telescope is not only dictated by the requirements of compactness inside the cryostat, but in a way that minimize the beam distortion at the output of the system [3].

In figure 1 we can see how the sky signal and LO signal are coupled to the mixer horn from the telescope FP and the LO feed respectively for both polarizations. The chief ray path from $M3$ (common to both configurations) to the antenna subreflector is following an off-axis trajectory since it has an inclination of $0.94°$ respect the telescope axis. This is due to the fact that the band 9 cryostat window is located off-axis in FP to accommodate the other ALMA channels. The $1P$ polarization beam path is a copy of the mirror system at the right side of the grid and rotated by $125°$ clockwise respect the incident point at the grid. The grid than works in reflection for the $1P$ polarization (linearly polarized on the plane of the $M3$ $M4$ ellipsoidal axis) and in transmission for the $0P$ polarization (orthogonally polarized respect $1P$). A beam splitter is located between $M4$ ($M4'$) and the mixer horn aperture with an inclination of $45°$ such as the linear polarized electric field is perpendicular to the plane of incidence. Another series of ellipsoidal mirrors, $M5$ ($M5'$) and $M6$ ($M6'$), are used to quasi-optically couple the LO signal source located at the $90K$ stage in the cryostat. The LO antenna is a diagonal horn. This kind of feed presents a optimum Gaussian beam coupling of $84\%$ that allows, with a proper beam guide, efficient power coupling with the mixer horn.

## III. Measurement setup

The measurement setup is a planar near-field antenna measurement based on radio heterodyne detection method using a vector network analyzer. Phase and intensity measures are then possible within the accuracies described in table I. Scan and optical mirror block alignment and parallelism are achieved by means of a theodolite in conjunction with well referenced point locations on the mirror block. In this way is then possible to establish a planarity (parallelism) relation within the scan stages and the mirror block. Autocollimation processes reflecting the theodolite laser beam, ensure parallelism. A set of cross-references drawn with know position on the mirror block to respect the $M3$ chief ray incident point, help to locate the source horn (held on the scan stages) in front of this incident point. By centering the scan to a set of 2 reference crosses aligned along the $X$ or $Y$ axis on the mirror block and reading the scan position, it is possible to fix the mirror block rotation around the $Z$ axis, setting its $Z$ tilt in order to correct rotation displacements. The precise alignment of the measurement system with the accuracies described in table I is difficult and the detailed information on the procedures used are not given in this paper.

## IV. Software model

Theoretical modelling and analysis were carried out by using different complementary techniques, from basic geometrical optical ray tracing, GBMA and vector field analysis with the commercial package GRASP8©. Ray tracing performed by means

TABLE I

MEASUREMENT SETUP FEATURES.

| Electrical properties | | |
|---|---|---|
| Gunn diode freq. | $[GHz]$ | $100 - 120$ |
| Multiplication chain, x2-x3 | [GHz] | $600 - 720$ |
| Output power | $[\mu W]$ | 60 |
| Dynamic range | $[dB]$ | $50 - 60$ |
| Detector | | Super Lattice Electronic Device |
| Amplitude stability | $[\%/hr]$ | $\pm 2$ |
| Phase stability | $[^{\circ}/hr]$ | $\pm 20$ |

| Scanner ranges and resolution | | |
|---|---|---|
| X,Y,Z travel ranges | $[mm]$ | 100 |
| Step accuracy | $[\mu m]$ | 5 |

| Alignment accuracy | | |
|---|---|---|
| X and Y offset | $[mm]$ | $\pm 0.1$ |
| Z offset | $[mm]$ | $\pm 0.2$ |
| X and Y rotations | $[^{\circ}]$ | $< 0.05$ |
| Z rotation | $[^{\circ}]$ | $< 0.1$ |

of ABCD law gives the essential information of a quasioptical system. From the optical design distances between objects in the system and single optical elements characteristics, such as focal length of the mirrors, slant length $R_h$ and aperture diameter of the corrugated horn, it is possible to describe how the fundamental Gaussian beam behaves along the optical path. For instance, radius $w$ and radius of curvature $R$ of the beam are traceable at each location between optical elements. The waist of the beam is than determined at each refocusing location depending on the frequency $f$. This technique treats the optical system as a paraxial system, without considering any diffraction effect due to truncations occurring at reflecting surfaces. Despite this limitations this method is a highly effective first order design and analysis tool. A more sophisticated software model can be implemented using GRASP8©. This is basically a software making use of Physical Optics (PO) approximations for the electromagnetic field computation. This technique allows to have vector information of the electromagnetic field in any location in the system under analysis. Its results are base on the full based Green's Maxwell equation solution considering the induced currents such as the electromagnetic field acts locally on the surface like a plane wave.The limits of applicability of this assumptions require scatters being large and smooth having a surface radius of curvature in terms of wavelength bigger than $6\lambda$. This is our case since all the mirrors were designed taking into account a minimum clearance of at least $5w$ as stated in section II. From experimental measurement comparisons and previous analysis using this software [4] it turned out that PO gives accurate results for the system being analyzed. Using one of the features of GRASP8©, mirror rims can be modelled on the basis of actual mirror production drawings. Therefore the evaluation of the electromagnetic field will produce high fidelity beam pattern, describing mirror edge diffraction. Grids and apertures in GRASP8© can also be analyzed allowing the evaluation of polarization and truncations effects respectively. Using GBMA a more detailed picture of the beam quality at the FP location can be obtained.

Particular attention has been paid to the description of the input field at the mixer horn aperture location. It has been seen that a simple Gaussian beam model of the horn electric field distribution with a proper waist, does not predict either the sidelobes and the main-beam distortions along the optical path. A better way to improve the input field is to assume the field at the corrugated horn aperture plane as a truncated Bessel function with a spherical phase front [7]. Despite this choice improved the quality of the simulated beams, there is still no information on the Cross-Polar (Xs-P) component at the horn aperture, since only the Co-Polar (Co-P) field is described by the truncated Bessel function. A further improved representation of the electric field at the horn aperture was achieved by applying mode matching techniques developed initially in [5] and expanded in [6]. The horn is regarded as a large number of waveguide sections in succession, which match the profile of the horn. Waveguide modes are tracked through the horn and power conserved. This technique has the advantage of describing Co-P and Xs-P at the aperture plane of a corrugated horn from the detailed mechanical drawings. Thus, we obtained a complete field description at each particular frequency of interest for the mixer horn. With this input field distribution the results from GRASP8© take also into account how the Xs-P level evolve along the optical path. As an example of accuracy of this model, coupling the Co-P component resulting from the procedure previously described, with a fundamental Gaussian at the horn aperture[1] at the frequency of $668GHz$, a Gaussian power coupling coefficient of $97.72\%$ was obtained. This value is very close to the model of a truncated Bessel function ($98\%$) given in [7].

[1]Virtual waist of $1.05mm$ inside the horn calculated at the frequency of $668GHz$.

## V. EXPERIMENTAL AND SOFTWARE DATA ANALYSIS

The aim of this section is to analyze beam electrical field distributions of the $0P$ and $1P$ beams at the FP from data obtained by real measurement and also software electromagnetic simulations. The measurement plane, both in the experiment set-up and in the software model, is a plane normal to the telescope axis with the center of the co-ordinate system located $145mm$ in front of the chief ray intersection point on $M3$ (see figure 1). In this frame the beams are coming parallel to the $Y-Z$ plane and with a slope of $0.94°$. By having the same measurement plane definition and relying on the measurement alignment accuracy, we can visually compare experimental and software set of data obtained at the scan location.

### A. E-Plane and H-Plane Field cuts comparisons

The comparisons between software and measured electric field patterns are shown in section VIII. The set of data presented here refers to both $0P$ (figures 2 and 3) and $1P$ (figures 4 and 5) polarization path at the two mentioned frequencies of 606 and $668GHz$. These plots represent intensity and phase at the E- and H-plane. Figure 7 refers to a measurement involving the beam passing through an aperture emulating the cryostat window and it will be explained in the end of this section. From these intensity and phase comparisons there is in general a good software and experimental data agreement in both phase and intensity distributions with high accuracy even at off-axis points from the main beam. This means that the measured beam is not diffracted by mechanical struts surrounding it. The five times the beam radius clearance design rule is respected along the whole optical path.

A particular measurement was carried out with the scanning source rotated at $45°$ to respect the two signal polarizations coming out from $M3$. In figure 6(a) and 6(b) the X and Y scan cuts are plotted on top of each other for a measurement at the frequency of $606GHz$. These plots show the two beams coming at the FP at the same location, indicating that the alignment of the two polarization signals is correct. At higher frequencies such behavior should be even better due to less diffraction effects and less phase front radius of curvature mismatches with the reflecting surfaces.

### B. Fundamental Gaussian beam mode analysis

A more qualitative analysis of the output beams could be made by means of GBMA. From the data distribution we can see how much the real beam is close to a fundamental Gaussian (fitting procedure), but also how much of the power of the real beam couples with the nominal fundamental Gaussian beam at the FP location. First we fit the field distribution with a fundamental Gaussian beam of unknown parameters. We carry out an overlap integral at the desired plane and vary the parameters of the Gaussian beam so as to maximize power coupling with the experimental or simulated field of interest. By maximizing the power coupling the equivalent Gaussian that best matches the field is obtained.

$$K = \left| \frac{\int_S E_m^* G ds}{\sqrt{\int_S E_m^* E_m ds \int_S G^* G ds}} \right|^2 \tag{1}$$

Equation (1) gives the amount of power coupled between the measured field $E_m$ and a fundamental Gaussian beam $G$. In general a fundamental Gaussian beam is described by a waist $w_0$ located in a certain point in the space. Additional displacement offsets along the 3 axis ($x_{Offset}$, $y_{Offset}$, $z_{Offset}$) and tilts in $x$ and $y$ ($\theta_x$ and $\theta_y$), give further degrees of freedom in order to define a beam in the space that best fit $E_m$. Considering the Gaussian distribution with a spherical phase front

$$\begin{aligned} G(x,y,z;w,R) \;=\; & \left(\frac{2}{\pi w}\right)^{0.5} \cdot \exp\left(-\frac{(x^2+y^2)}{w^2}\right) \cdot \\ & \cdot \exp\left(-j\pi\frac{(x^2+y^2)}{\lambda R}\right) \cdot \\ & \cdot \exp(j\phi_0) \cdot \exp\left(-j\frac{2\pi z}{\lambda}\right) \end{aligned} \tag{2}$$

where beam radius $w$, radius of curvature $R$ and phase shift $\phi_0$ depend on $z$ [7], it is possible to include displacement and tilts of the plane wave phase front term (i.e. the beam direction) by using the following projections

$$x' = x_{Offset} + x\cos\theta_x \tag{3}$$

$$y' = y_{Offset} + y\cos\theta_y \tag{4}$$

$$z' = z_{Offset} + x\sin\theta_x + y\sin\theta_y \tag{5}$$

Using this projection we can move the fundamental Gaussian and also varying the waist $w_0$, to maximize power coupling (1). If displacements, tilts and waist are left free to vary and we apply the maximization of $K$, we obtain a set of these parameters describing which is the fundamental Gaussian beam that best fits $E_m$. In table II and III the results of this procedure are

TABLE II

FUNDAMENTAL GBMA AT $606GHz$

| $f = 606GHz$ | Experimental | | Software | | Expected |
|---|---|---|---|---|---|
| | $0P$ | $1P$ | $0P$ | $1P$ | |
| Gaussucity, $[\%]$ | 98.15 | 98.31 | 98.19 | 97.99 | $\sim$ 98 |
| $w_0$, $[mm]$ | 3.00 | 2.95 | 2.98 | 2.98 | 2.96 |
| $x_{Offset}$, $[mm]$ | 0.06 | 0.26 | 0.00 | -0.10 | 0.00 |
| $y_{Offset}$, $[mm]$ | 2.58 | 2.85 | 2.45 | 2.45 | 2.47 |
| $\theta_x$, $[^\circ]$ | 0.06 | -0.04 | 0.00 | 0.14 | 0.00 |
| $\theta_y$, $[^\circ]$ | 1.00 | 0.88 | 0.99 | 0.99 | 0.94 |

TABLE III

FUNDAMENTAL GBMA AT $668GHz$

| $f = 668GHz$ | Experimental | | Software | | Expected |
|---|---|---|---|---|---|
| | $0P$ | $1P$ | $0P$ | $1P$ | |
| Gaussucity, $[\%]$ | 98.56 | 98.66 | 98.16 | 97.97 | $\sim$ 98 |
| $w_0$, $[mm]$ | 2.82 | 2.74 | 2.70 | 2.70 | 2.67 |
| $x_{Offset}$, $[mm]$ | 0.10 | 0.28 | 0.00 | -0.09 | 0.00 |
| $y_{Offset}$, $[mm]$ | 2.58 | 2.86 | 2.44 | 2.44 | 2.46 |
| $\theta_x$, $[^\circ]$ | 0.06 | 0.02 | 0.00 | 0.13 | 0.00 |
| $\theta_y$, $[^\circ]$ | 1.02 | 0.94 | 0.98 | 0.98 | 0.94 |

shown for the two measured and simulated data set at 606 and $668GHz$. If instead we consider what the ideal beam should be at the FP location, we find the power coupling efficiency between $E_m$ and $G$. By setting the offsets in such a way they describe the nominal fundamental Gaussian beam at the FP for a certain frequency, we obtain coupling efficiencies shown in table IV. The values of waist at the FP come from the ABCD analysis at the chosen frequencies. However if we leave only $z_{Offset}$ free to vary, we found a value of $z_{Offset}$ that tell us what is the defocusing along the telescope axis, of $E_m$ with respect to the location of the nominal fundamental Gaussian at the FP waist position. In table V we list the defocusing of the measured and simulated beams at the FP. Such levels of defocuosing are not be worrying since as pointed out in [3], by means of repositioning the secondary mirror of the Cassegrain system, it is possible to bring the efficiency back to optimal levels.

### C. Cryostat window effects

One of the big concerns in coupling the feed beam with the telescope is in fact its passage through the cryostat window. This window usually has to be as small as possible to avoid scattering of ambient temperature radiation into the receiver. As a first attempt to investigate the effects of the cryostat window we carried out a measurement with a circular aperture at the cryostat window location. The aperture diameter was $20mm$ and centered $150mm$ from $M3$ chief ray intersection point. In figure 7 is shown the comparison between experimental measurement and software result for the $1P$ polarization, obtained introducing such kind of aperture in the GRASP8© model. Despite the simplified experiment, it is clear that the window aperture in itself does not introduce noticeable diffraction effects on the main beam.

TABLE IV

COUPLING WITH THE NOMINAL GAUSSIAN AT THE FP, $[\%]$

| $f$, $[GHz]$ | nominal $w_0$, $[mm]$ | Experimental | | Software | |
|---|---|---|---|---|---|
| | | $0P$ | $1P$ | $0P$ | $1P$ |
| 606 | 2.96 | 97.84 | 95.90 | 98.14 | 97.65 |
| 668 | 2.67 | 97.73 | 95.46 | 98.11 | 97.64 |

TABLE V

DEFOCUSING AT THE FP, $[mm]$

| $f$, $[GHz]$ | Experimental | | Software | |
|---|---|---|---|---|
| | $0P$ | $1P$ | $0P$ | $1P$ |
| 606 | 1.4 | 1.7 | 1.6 | 0.3 |
| 668 | -1.4 | -0.3 | 1.1 | 0.1 |

## VI. LO POWER BUDGET

One of the features of GRASP8© is the ability to give the power spill-over efficiency at each of the scatters through the signal path. The Co-P linear polarized electric field at the LO diagonal horn aperture plane using equation (7.52) of [7]. Propagating this field from the diagonal horn aperture through $M4$, $M5$ and the Beam Splitter (BS) we obtain the total path spill-over and the field distribution of the LO signal at the mixer horn aperture. The BS is a thin slab of Mylar ($13\mu m, n = 1.73$). The power reflection coefficient was calculated at the frequencies of 600, 660, $720GHz$ (average of $6\%$), considering that the LO signal is perpendicular to the plane of incidence. Thus after spill-over and reflection at the BS, the LO signal reaches the mixer horn aperture with a certain aperture efficiency. Finally, with an average LO power at the diagonal horn aperture of $40\mu W$, we show in table VI what is the level of LO power arriving at the mixer horn aperture. These power levels are sufficiently high to pump the mixer, since its minimum power level requirement is about $0.5\mu W$. Furthermore, slight misalignments of the LO optics could be also tolerated. The data shown in table VI do not include coupling inside the mixer.

TABLE VI

TOTAL LO POWER REACHING THE MIXER HORN WITH $40\mu W$ INPUT POWER. [$\mu W$]

| $f$, [$GHz$] | $0P$ | $1P$ |
|---|---|---|
| 600 | 1.84 | 1.84 |
| 660 | 2.21 | 2.21 |
| 720 | 2.61 | 2.61 |

## VII. FURTHER WORK AND CONCLUSION

In this paper we analyzed the optical coupling system for the ALMA band 9 front-end. Experimental and simulated data agree very well. The field distribution (both intensity and phase) have been calculated and compared for the two polarization configurations. From visual comparison it is evident that the measured beams does not suffer from mechanical strut diffraction effects, since the beam shapes resemble the simulated ones. A fundamental Gaussian beam mode analysis was carried out, indicating that the beams are behaving as expected, maintaining a good level of power coupling efficiency with the nominal fundamental Gaussian at the FP. A slight defocusing effect was illustrated, but within the range of tolerance which can be corrected by movement of the secondary along the telescope axis. The LO beam guide was analyzed to deduce the level of LO signal power effectively reaching the mixer horn aperture. The overall analysis shows that the optical coupling system is working properly respecting the design specification in order to be coupled with the Cassegrain antenna. It was not shown here, but it has been seen that both $0P$ and $1P$ signals are reaching the secondary with the required edge taper of $12dB$, as well as a cross-polar level at the FP less than $20dB$. Further analysis of the beams with the receiver at cryogenic temperatures (such as orthogonality of the two polarizations and coupling with the telescope, will be part of the next phase of work in assessment of the ALMA band 9 optical front-end.

## VIII. Software and experimental comparison plots

### A. 0P polarization

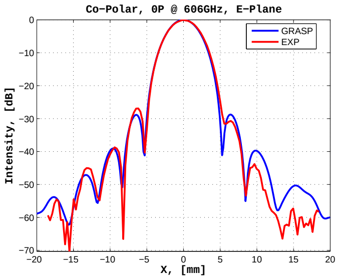


(a) Intensity, E-Plane

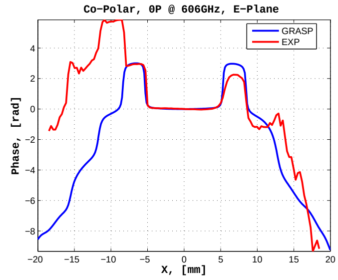


(b) Phase, E-Plane

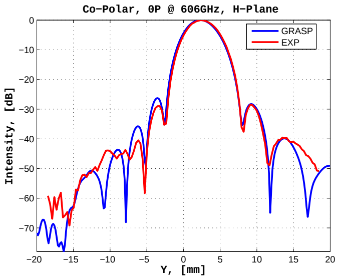


(c) Intensity, H-Plane

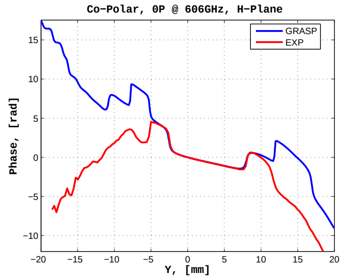


(d) Phase, H-Plane

Fig. 2. Experimental and software data comparison of the $0P$ polarization signal at $606GHz$. Intensity and phase at E- and H- plane. Measured plane at $145mm$ from the chief ray incident point on $M3$.

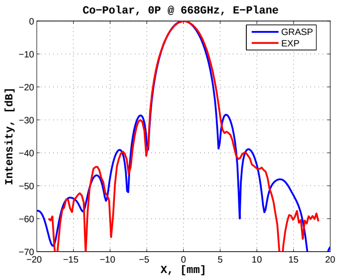


(a) Intensity, E-Plane

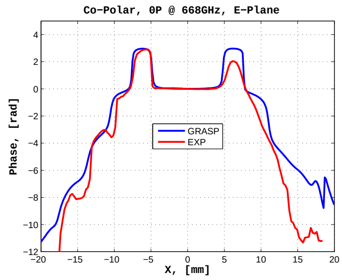


(b) Phase, E-Plane

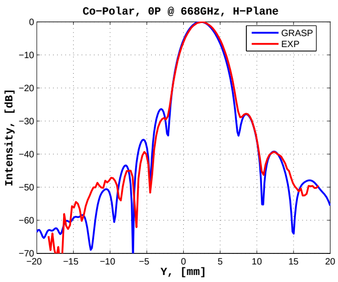


(c) Intensity, H-Plane

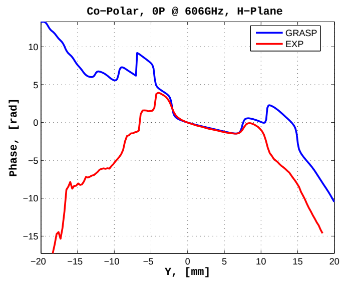


(d) Phase, H-Plane

Fig. 3. Experimental and software data comparison of the $0P$ polarization signal at $668GHz$. Intensity and phase at E- and H- plane. Measured plane at $145mm$ from the chief ray incident point on $M3$.

## B. 1P polarization

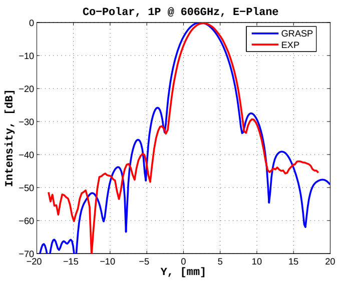


(a) Intensity, E-Plane

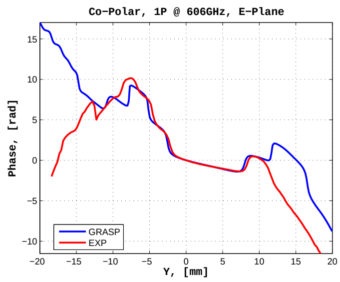


(b) Phase, E-Plane

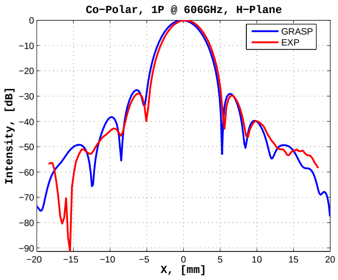


(c) Intensity, H-Plane

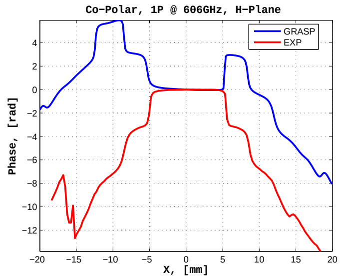


(d) Phase, H-Plane

Fig. 4. Experimental and software data comparison of the $1P$ polarization signal at $606GHz$. Intensity and phase at E- and H- plane. Measured plane at $145mm$ from the chief ray incident point on $M3$.

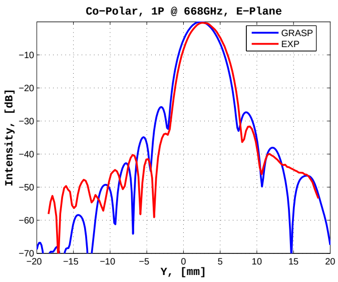


(a) Intensity, E-Plane

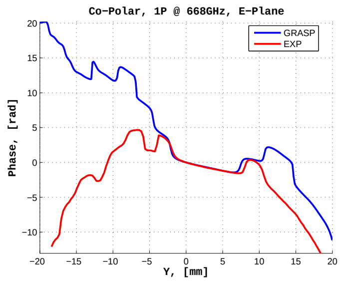


(b) Phase, E-Plane

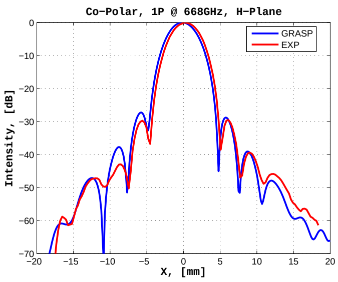


(c) Intensity, H-Plane

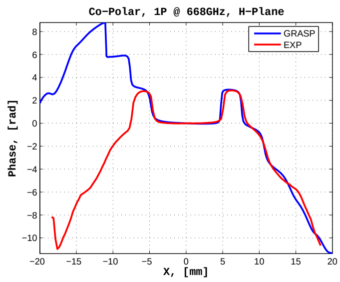


(d) Phase, H-Plane

Fig. 5. Experimental and software data comparison of the $1P$ polarization signal at $668GHz$. Intensity and phase at E- and H- plane. Measured plane at $145mm$ from the chief ray incident point on $M3$.

## C. 45° measurement comparison

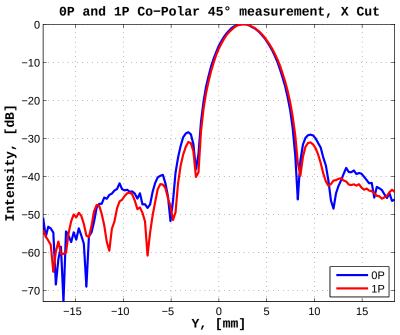


(a) X Cut

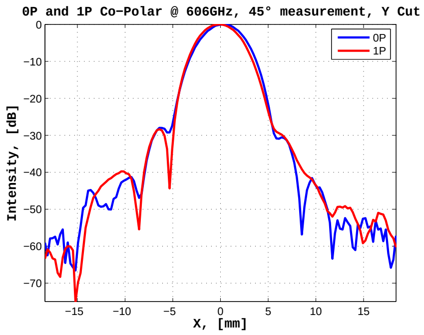


(b) Y Cut

Fig. 6. Experimental 45° measurement comparison.

## D. Cryostat aperture emulation

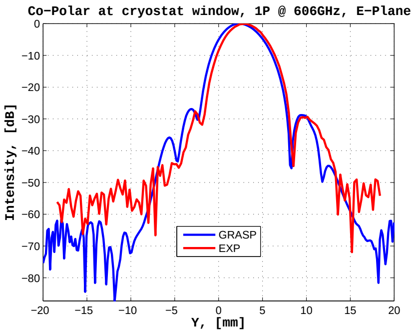


(a) Intensity, E-Plane

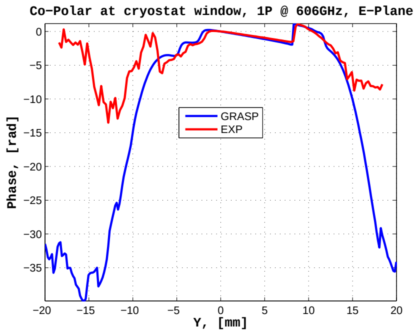


(b) Phase, E-Plane

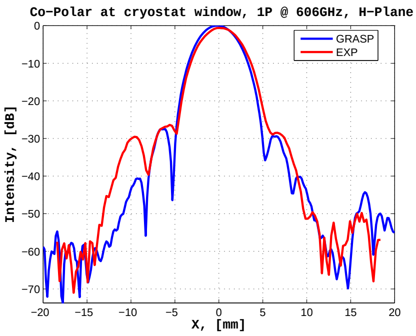


(c) Intensity, H-Plane

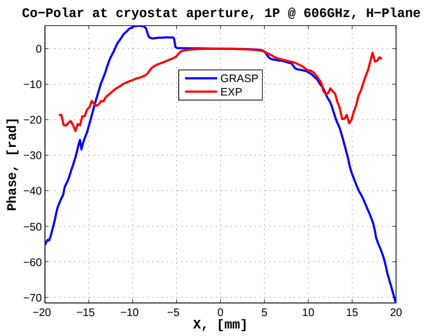


(d) Phase, H-Plane

Fig. 7. Experimental and software data comparison of the $1P$ polarization signal at $606GHz$ after passing through the Cryostat window. Intensity and phase at E- and H- plane. Measured plane at $155mm$ from the chief ray incident point on $M3$.

## ACKNOWLEDGMENT

The authors would like to thank B. D. Jackson for his advice and helpful input throughout the measurement and verification phase of Band 9 front-end optics. This research was financed by the European Southern Observatory (ESO) (contract number: 73072/MAP/03/8632/GWI).

## REFERENCES

[1] A. Baryshev, M. Carter, W. Jellema, R. Hesper, *Design and evaluation of ALMA band 9 quasi-optical system*, Proc. of the $5^{th}$ Int. Conf. on Space Optics, 30 March - 2 April 2004, Toulouse, France. Ed.: B. Warmbein. ESA SP-554, Noordwijk, NetherlandsL ESA Publication Division, ISBN 92-9092-865-4, p. 365-371.

[2] A. Baryshev, M. Carter, M. Candotti, N. A. Trappe, J. A. Murphy, *Verification of the optical design for band 9 of the ALMA receiver*, Proceedings of the $29^{th}$ Int. Conf. on Infrared and Millimeter Waves and $12^{th}$ Int. Conf. on THz Electronics, Univ. of Karlsruhe, Karlsruhe (Germany), Sep. 27 - Oct. 1, 2004.

[3] A. Baryshev, W. Wild, *ALMA band 9 optical layout*, ALMA Memo 394, September 2001.

[4] M. Candotti, G. Cahill, T. Finn, W. Jellema, J. Lavelle, J. A. Murphy, C. O'Sullivan, N. A. Trappe, *Quasi-Optical Verification of the Focal Plane Optics of the Heterodyne Instrument for the Far-Infrared (HIFI)*, Proc. of the SPIE Astronomical Telescopes and Instrumentation Symposium, 21 - 25 June 2004, Glasgow, Scotland (UK).

[5] A. D. Olver,P. J. B. Clarricoats, A. A. Kishk and L. Shafai, *Microwave Horns and Feeds*, IEEE Press, 1994.

[6] J. A. Murphy, R. Colgan, C. O'Sullivan, B. Maffei, P. Ade, *Radiation patterns of multi-moded corrugated horns for far-IR space applications*, Infrared Physics and Technology, Vol. 43, p. 515 - 528, 2001.

[7] P. F. Goldsmith, *Quasioptical Systems: Gaussian beam quasioptical propagation and applications*, IEEE Press, New York, 1997.